

## Dry and wet granular shock waves

V. Yu. Zaburdaev\* and S. Herminghaus†

*MPI for Dynamics and Self-Organization, Bunsenstrasse 10, 37073 Göttingen, Germany*

(Received 24 August 2006; revised manuscript received 17 January 2007; published 12 March 2007)

The formation of a shock wave in one-dimensional granular gases is considered, for both the dry and the wet cases, and the results are compared with the analytical shock wave solution in a sticky gas. Numerical simulations show that the behavior of the shock wave in both cases tends asymptotically to the sticky limit. In the inelastic gas (dry case) there is a very close correspondence to the sticky gas, with one big cluster growing in the center of the shock wave, and a steplike stationary velocity profile. In the wet case, the shock wave has a nonzero width which is marked by two symmetric heavy clusters performing breathing oscillations with slowly increasing amplitude. All three models have the same asymptotic energy dissipation law, which is important in the context of the free cooling scenario. For the early stage of the shock formation and asymptotic oscillations we provide analytical results as well.

DOI: [10.1103/PhysRevE.75.031304](https://doi.org/10.1103/PhysRevE.75.031304)

PACS number(s): 45.70.-n, 47.40.-x, 45.50.-j

### I. INTRODUCTION

There are three distinct elaborated models for dissipative gases, which find direct and fruitful applications in many physical systems. These are the sticky, the inelastic, and the wet granular gas. The first two have been thoroughly studied for decades (see Refs. [1–7] for the inelastic and [8–12] for the sticky gas). Their applications span from dry granular matter research to the description of large scale structure formation in the universe. The wet granular gas model is still quite young, but nevertheless its intimate connection to the former two models has already been proven [13,14].

In all three models, particles collisions are dissipative, but conserve the total momentum and mass. Moreover, it has been demonstrated recently that during free cooling these models share the same asymptotic behavior [14,15]. This asymptotic regime is known as a “sticky limit” [16,17]. For the free cooling of a one-dimensional sticky gas, its total energy decays in time as  $E(t) \simeq \gamma t^{-2/3}$  [12]. Although this result can be obtained from simple scaling estimates, its rigorous derivation is not trivial. It was proven that the dynamics of a gas of particles, which stick together upon contact and conserve momentum and mass, is equivalent to the dynamics of shock waves in the inviscid Burgers equation for velocities [9,18,19]. The energy dissipation in the Burgers equation with random initial data was known already for some time [20]. The same analogy made it possible to find the mass and the velocity distribution functions analytically in a free cooling sticky gas [10,11].

Shock waves develop in the asymptotic regime of the inelastic gas as well [16], and a similar behavior is found for the wet gas. Currently, different hydrodynamic and kinetic approaches are actively discussed in the literature, aiming to describe the physics of the free cooling and driven granular gases, including shock wave phenomena [21–29]. They involve a number of rich and complicated issues, such as the clustering instability, large gradients in density and velocity,

inelastic collapse, etc. [30–35]. Therefore prior to the analysis of the complex behavior of a set of shock waves, explicit knowledge of the individual shock can be extremely helpful. In the present paper, we investigate such individual shocks in one-dimensional inelastic and wet granular gases, and show how they relate to the well-known sticky limit. We must note, however, that the one-dimensionality of the problem imposes a limitation on the applicability of the results. One has to be careful extending the conclusions to higher dimensions.

The structure of the paper is as follows. In the next section we briefly describe peculiarities of all three models. We also discuss conservation laws and, following from them, the pressureless gas dynamics system of equations. The analytical solution for the shock wave in the sticky gas is reproduced. With its help we formulate our problem setup. In the third section, we present numerical results for the simulation of an individual shock wave in the inelastic gas. The fourth section contains analytical results concerning the early stage of the shock formation. The fifth section is devoted to the shock wave in a wet gas. It is followed by Sec. VI, where a theoretical toy-model for the asymptotic behavior of the wet shock wave is presented. The last section is reserved for conclusions.

### II. THREE INELASTIC GAS MODELS

We start by presenting a general setup of the problem, and by giving a brief description of all three models and their common properties. Consider a one-dimensional system of pointlike particles. Take two collision partners with velocities  $v_1, v_2$  and masses  $m_1, m_2$ . In a dissipative collision these two particles lose energy. In the sticky case [8], they just stick together losing all their relative kinetic energy  $\mu(v_1 - v_2)^2/2$ , where  $\mu = m_1 m_2 / (m_1 + m_2)$  is the reduced mass. They continue their motion as a single particle with mass  $m_1 + m_2$  and a center of mass velocity  $v_{\text{CM}} = (m_1 v_1 + m_2 v_2) / (m_1 + m_2)$ , thus conserving the total momentum and mass.

In a more general situation of the one-dimensional inelastic gas [2], they lose a fixed fraction of their relative kinetic

\*Electronic address: [vasily.zaburdaev@ds.mpg.de](mailto:vasily.zaburdaev@ds.mpg.de)

†Electronic address: [stephan.herminghaus@ds.mpg.de](mailto:stephan.herminghaus@ds.mpg.de)

energy. Therefore the magnitude of their relative velocity is reduced by a factor  $\epsilon$ :  $|v_1 - v_2| \mapsto \epsilon|v_1 - v_2|$ . The coefficient of restitution,  $\epsilon$ , varies from the completely inelastic (sticky) limit,  $\epsilon=0$ , to perfectly elastic collisions,  $\epsilon=1$ .

The wet granular gas model is somewhat more complex [13]. In a wet gas, each particle (for a moment we imagine it to be a spherical perfectly elastic particle with finite radius) is covered with a thin liquid film. In a real granular system this film can appear as a result of humidity, or simply because some liquid was deliberately added into a sample. When such particles come into a contact, a liquid bridge forms between them. As they start to move apart, the liquid bridge extends and acts as an attractive force between the particles. At some critical distance the liquid bridge ruptures and liberates the particles. The energy required to rupture the liquid bridge depends on the liquid properties and on the volume of the liquid in the bridge. For a given liquid content, this energy may be considered constant and will be denoted by  $E_{\text{loss}}$ . It defines a threshold selecting one of two possible outcomes of a collision between two wet particles. They either rupture the liquid bridge losing the fixed amount of energy  $E_{\text{loss}}$ , or they stay bound by the liquid bridge and continue their motion as a pair. In what follows, we adopt a simpler model which mimics the behavior discussed above. We assume the whole process of bridge formation and rupture to be a single event (i.e., pointlike in time and space), and characterized solely by  $E_{\text{loss}}$ . If the relative kinetic energy of the particles is above  $E_{\text{loss}}$ , they move apart after the collision with conserved total momentum and the total kinetic energy reduced by the amount  $E_{\text{loss}}$ . If they are slow enough ( $|v_1 - v_2| < \sqrt{2E_{\text{loss}}/\mu}$ ), they just stick together like in the sticky gas and lose all of their relative kinetic energy.

In our attempt to describe the above models in a hydrodynamical way we may use the two conservation laws, namely the conservation of mass and momentum. In the simplest case they can be written in the form of the pressureless gas dynamic system (for the discussion of its applicability see below)[36]:

$$\begin{aligned} \partial_t \rho + \partial_x(\rho u) &= 0, \\ \partial_t(\rho u) + \partial_x(\rho u^2) &= 0, \end{aligned} \quad (1)$$

where  $\rho(x, t)$  is the density of particles and  $u(x, t)$  is their macroscopic velocity field. Indeed, in the momentum current in the second equation of Eq. (1) the pressure term is absent. This approximation works well for the sticky gas and for the limiting regime of the inelastic gas, when the granular temperature tends to zero. In the general case, the pressure term must appear, which is a complicated issue for dissipative gases. In order to have a self-consistent expression for the pressure, the complete set of kinetic equations must be written down and averaged, and this appears to be a difficult task even for the inelastic gas [26].

The above system of equations (1) deserves far more attention than we are able to devote to it in this paper. We mention just a few of its remarkable properties. First of all, it is easy to see that formally the system (1) gives the Hopf equation for the velocity [37]:

$$\partial_t u + u \partial_x u = 0. \quad (2)$$

Often in the literature it is presented in the form of the inviscid Burgers' equation [20,38],

$$\partial_t u + u \partial_x u = \nu \partial_{xx}^2 u, \quad \nu \rightarrow 0, \quad (3)$$

which has a wide range of applications [39–42]. Despite its nonlinear form it is exactly solvable with the use of the Hopf-Cole transformation,  $u = -2\nu \partial_x \ln \psi$ , which transforms it to the classical diffusion equation for  $\psi$ .

Hopf's and Burgers' equations have solutions in the form of shock waves. A negative velocity gradient, if present in the initial velocity profile, steepens until it becomes vertical. In the Hopf equation, the solution becomes discontinuous in a finite time. After that one has to deal with weak (discontinuous) solutions of this equation. In the Burgers equation, the nonlinear steepening is finally balanced by the viscosity term which sets in at large velocity gradients. It was proven that the free cooling scenario of the sticky gas corresponds to the dynamics of shock waves in the inviscid Burgers' equation, and the merging of clusters is equivalent to the collision rules for shock waves [9].

It should be noted that the above pressureless gas system (1) has a weak solution (measure solution) in the form of the finite system of colliding particles [18,36]. It corresponds to the discrete finite set of Dirac delta-functions in the initial conditions for the density and velocity. It is remarkable that such measure solutions of Eq. (1) exist for *all three types* of collisions conserving momentum and mass (for the proof see [36]). That is why we have chosen the pressureless gas dynamic system as a starting point for our consideration. In order to have a unique solution, an additional condition should be included, such as, for example, an appropriate collision rule. However, in the "hydrodynamic" limit, when the number of particles tends to infinity with bounded total mass and initial velocities, the existence and uniqueness of a measure solution with a proper entropy condition was proven *only* for the sticky collision rules [9,18]. In the sticky case, weak solutions of the pressureless system with the sticky collision rule are equivalent to the weak solutions of the inviscid Burgers' equation. The viscosity term on the right-hand side of the Burgers' equation automatically gives the sticky merging of colliding shocks. What happens in the remaining two cases of inelastic and wet granular gases remains an open mathematical problem [18]. It is only clear that in the case of inelastic and wet granular gas weak solutions of Eq. (1) will not be weak solutions of Burgers' equation.

Here we are interested in the behavior of an individual shock wave. Consider two domains of the one-dimensional gas which occupy the left and right halves of the  $x$  axis. At the beginning they have arbitrary but spatially constant densities and opposite velocities. Essentially this is the starting point for the collision of two rows of gases with different densities (Riemann problem [36]):

$$\rho(x, 0) = \begin{cases} \rho_l & \text{if } x < 0, \\ m_0 \delta(x) & \text{if } x = 0, \\ \rho_r & \text{if } x > 0, \end{cases}$$

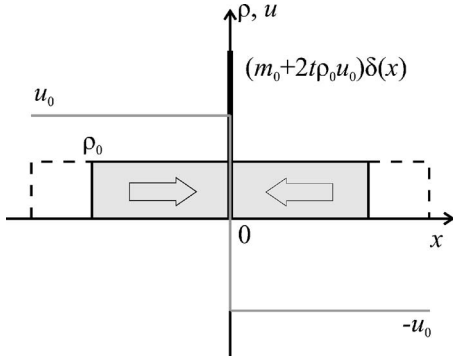


FIG. 1. Weak solution of the pressureless gas dynamics system corresponding to the sticky gas model. The velocity profile denoted by a gray line is stationary. Particles from the dashed areas are accumulated in the delta peak in the center.

$$u(x,0) = \begin{cases} u_l & \text{if } x < 0, \\ u_c & \text{if } x = 0, \\ u_r & \text{if } x > 0, \end{cases}$$

where  $\rho_l, \rho_r, m_0 > 0$ ;  $u_l \geq u_c \geq u_r$ ,  $u_l > u_r$ . For the case of sticky particles and the Hopf equation, the density and velocity evolution can be easily found. For simplicity we take a symmetric case, when  $\rho_l = \rho_r = \rho_0$  and  $u_l = -u_r = u_0$ ,  $u_c = 0$ . Then, the weak solution of the sticky gas will be (see Fig. 1)

$$\rho(x,t) = \begin{cases} \rho_0 & \text{if } x < 0, \\ (m_0 + 2t\rho_0|u_0|)\delta(x) & \text{if } x = 0, \\ \rho_0 & \text{if } x > 0, \end{cases}$$

$$u(x,0) = \begin{cases} u_0 & \text{if } x < 0, \\ 0 & \text{if } x = 0, \\ -u_0 & \text{if } x > 0. \end{cases}$$

The two rows experience a head-on collision, and at the collision point a big cluster grows. The mass of this cluster increases linearly with time, and the velocity profile remains stationary.

For the inelastic gas there are no equations at hand, which could describe its hydrodynamics in the regime of divergent densities and steep velocity profiles (see, however, [26]). For the wet gas, only the first steps have been taken in this direction, and the whole hydrodynamic approach still needs to be developed. This is why we address this problem with the help of numerical simulations. However, microscopic analysis of the shock allows us to obtain some analytical results for the early and late stages of the shock wave development as well.

### III. INELASTIC GAS (NUMERICAL RESULTS)

To begin, we consider the results of numerical simulations of a collision of two equal rows of equidistantly spaced identical pointlike particles with opposite velocities. The total number of particles is  $N$ . If two inelastic particles with a restitution coefficient  $\epsilon$  and initial velocities  $v_1, v_2$  collide

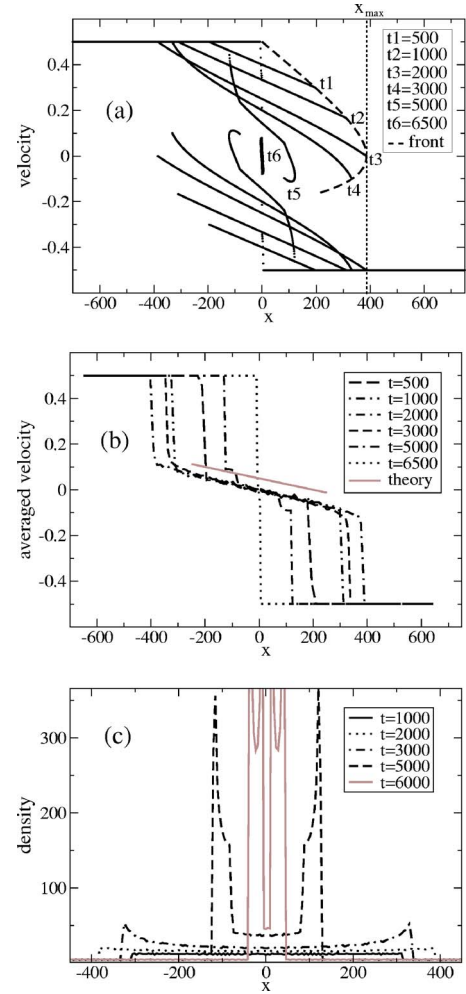


FIG. 2. (Color online) Simulations of a shock wave in the inelastic gas ( $u_0 = \pm 0.5$ ,  $l = m = 1$ ,  $\epsilon = 0.999$ ,  $N = 8000$ ,  $\delta = 10^{-5}$ ). (a) Velocities of particles at different times, the dashed line corresponds to the trajectory of the wave front [Eqs. (4) and (5)]. (b) Averaged velocity profiles, the gray line indicates the slope predicted by theory [Eq. (6)]. (c) The density of particles (not normalized).

with each other, their postcollision velocities will be  $v'_1 = v_1 - (1 + \epsilon)(v_1 - v_2)/2$  and  $v'_2 = v_2 + (1 + \epsilon)(v_1 - v_2)/2$ , respectively. The relative velocity of the particles changes its sign and is reduced by the factor  $\epsilon$ . However, it might be easier to give a slightly different interpretation. Because all of the particles are identical, we can imagine that they just pass one through another (instead of being reflected) and decelerate due to the inelasticity of the collision. Thus we can say that one row of particles interpenetrates into the other one, and the shock wave collision front forms.

In Fig. 2 we present the numerical results from simulations of the shock wave in the inelastic gas. The initial distance between particles gives the typical spatial scale of the problem and is set to unity:  $l = 1$ . For particles with unit mass,  $m = 1$ , the initial density is given by  $\rho_0 = m/l = 1$ . The initial velocity of the rows is  $\pm 0.5$ , so that their relative velocity is one,  $v_{\text{rel},0} = 1$ . Thus the typical time scale is also equal to one,  $t_0 = l/v_{\text{rel},0} = 1$ . In the following figures all corresponding quantities are considered to be dimensionless:

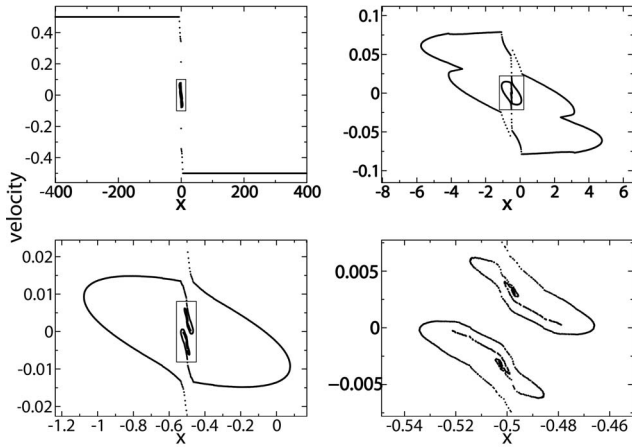


FIG. 3. Self-similar structures of velocities in the late stage of the shock wave formation ( $t=6500$ , all other parameters are the same as in Fig. 1). Rectangular boxes denote consequent zoom-in areas. The asymmetry in the final stage is due to the initially perturbed particle positions.

$x \rightarrow x/l$ ,  $v \rightarrow v/v_{\text{rel},0}$ ,  $\rho \rightarrow \rho/\rho_0$ ,  $t \rightarrow t/t_0$ , and  $E \rightarrow E/mv_{\text{rel},0}^2$ . The restitution coefficient is chosen as  $\epsilon=0.999$  in order to have a reasonable number of particles involved in the shock and to provide satisfactory statistics. In the simulations we use an event driven algorithm which utilizes the heap structure for sequencing the collision events. In order not to create additional difficulties for the heap with simultaneous collisions due to the initial symmetry of the problem, we perturb slightly the initial positions of particles. To avoid the appearance of the inelastic collapse we use the same strategy as in Ref. [16], where inelastic collisions below some threshold velocity,  $\delta$ , were substituted by perfectly elastic collisions. It was also shown there (and we checked it as well) that results did not depend on the threshold parameter  $\delta$ , provided it was small enough. We set it to be  $\delta=1 \times 10^{-5}$ .

In Fig. 2(a) we plot the velocities of single particles at different times (therefore these are not lines, but dense sets of single points). We can see that on the early stage of the process two rows penetrate into each other with an almost linearly decreasing velocity. As time increases, the particles on the penetration front slow down to zero velocity and change their direction motion. Thus one can speak of a final penetration depth of the shock wave. From this maximal width, the shock wave is compressed almost to a single point by the constantly approaching particles from both sides. The numerics allowed us to zoom into this point and revealed an extremely complex self-similar structure (see Fig. 3). The final stage of the shock wave development coincides with that of the sticky gas: one big cluster of particles is formed in the center of the shock wave.

The number of particles in this cluster grows linearly with time because each particle hitting it from either of the sides gives away all its momentum to the particles of the cluster and joins (“stick to”) it. The same mechanism is responsible for the sticking of inelastic clusters in a free cooling gas [16]. However, with an elastic cutoff at low velocities it is impossible to go further with numerics. The density of particles becomes so high that even double precision is not enough to

resolve their positions. This problem could be circumvented only by introducing sticky collisions instead of elastic ones, but that would substitute the original nature of sticking in the model.

In Fig. 2(b) we plot the average velocity of particles. Averaging was performed with different sizes of the averaging interval in order to check that sampling does not effect the results. In the current plot, average velocity profiles have 25–50 points inside the shock region. The initial stage is quite remarkable, where a constant negative velocity slope is preserved in time. This clearly demonstrates the inapplicability of the Hopf equation for the description of the Riemann problem of the shock wave in the inelastic gas. In the Hopf equation, each profile with a negative slope must come to turnover, whereas in the inelastic gas it conserves its slope, which is still true even for some time after the motion of the front is reversed.

The density of particles is shown in Fig. 2(c). At the early linear stage, a steplike uniform perturbation of density grows. In the perfectly elastic case this density would be just twice the density of a row, but in the inelastic case it is larger. Due to the dissipation, the velocity of the front propagation is smaller than the velocity of rows, and this leads to the accumulation of particles. As the propagation front slows down, more particles are collected at the borders. When the velocity of the front reverses, new incoming particles compress those in the interaction front and push them to the center: high density peaks start to grow. At a later stage of the process, these peaks can break into finer structures (secondary refraction waves). In the final asymptotics, the density peaks collapse into a single cluster. It is remarkable that quantities such as the trajectory and the maximal front width (penetration depth of rows), the slope of the mean velocity, and growth of the density profile in the linear stage can be obtained analytically from microscopic considerations. These will be presented next.

#### IV. INELASTIC GAS (ANALYTICAL RESULTS)

We start by tracing the very first particle with a velocity  $u_0 > 0$ , running from left to right into (and through) a row of equidistant particles with opposite velocities  $-u_0$ . By using the inelastic collision rules it is possible to connect the velocities, coordinates and times of the collisions of two successive interactions  $n$  and  $n+1$ :

$$u_{n+1} = u_n \frac{1+\epsilon}{2} - u_0 \frac{1-\epsilon}{2},$$

$$x_{n+1} = x_n + u_n dt_n,$$

$$dt_n = l/|u_n + u_0|,$$

where  $l$  is a distance between two neighboring particles ( $l = \rho_0^{-1}$ ). From these equations we can find the general dependence of the sequence on the step number,  $n$ :

$$u_n = u_0 \left[ 2 \left( \frac{1+\epsilon}{2} \right)^n - 1 \right];$$

$$x_n = x_0 + nl - \frac{l}{2} \frac{1 - \left(\frac{2}{1+\epsilon}\right)^n}{1 - \left(\frac{2}{1+\epsilon}\right)};$$

$$t_n = \frac{l}{2u_0} \frac{1 - \left(\frac{2}{1+\epsilon}\right)^n}{1 - \left(\frac{2}{1+\epsilon}\right)}.$$

In doing so we assume that the restitution coefficient is not too small, such that a reasonable number of collision events could occur before the particle changes its direction of motion. Here  $x_0$  is the center of the shock wave, and below we set it to zero. Expressing now the collision number as an inverse function of time we can write the time dependence of the velocity,  $u_f(t)$ , and the coordinate,  $x_f(t)$ , of the right front of the shock wave:

$$u_f(t) = u_0 \left( \frac{2}{1 + \frac{2u_0 t}{l} \left( \frac{1-\epsilon}{1+\epsilon} \right)} - 1 \right); \quad (4)$$

$$x_f(t) = l \frac{\ln \left( 1 + \frac{2u_0 t}{l} \left( \frac{1-\epsilon}{1+\epsilon} \right) \right)}{\ln 2 - \ln(1+\epsilon)} - u_0 t. \quad (5)$$

In Fig. 2(a) we plot the trajectory of the front (dashed line). We see that it agrees perfectly with numerical simulations until the first collision with a particle inside the interaction front appears. This happens only after the front has stopped expanding and has turned around to collapse. This is why we can find the turnover time by setting the front velocity (4) equal to zero. Inserting the turnover time in the expression for the coordinate (5), we find the maximal front width,  $x_{\max}$ , as a function of the interparticle distance (or density) and the restitution coefficient:

$$x_{\max} = l \left[ \frac{\ln 2}{\ln \frac{2}{1+\epsilon}} - \frac{1}{2} \left( \frac{1+\epsilon}{1-\epsilon} \right) \right].$$

Note that the penetration depth does not depend on the relative velocity of the rows.

Using the information about the front position and a linear approximation for the velocity and density profiles, we can find the slope of the average velocity in Fig. 2(b). For this purpose, we assume that the density of particles moving from left to right (from right to left) linearly increases (decreases) from the left to the right border of the interaction area. The total density of particles in the interaction area is spatially constant [cf. Fig. 2(c)]. The height of the density plateau in this stage,  $\rho_{\text{int}}$ , is governed by the simple relation  $\rho_{\text{int}} = \rho_0 + \rho_0 u_0 t / x_f(t)$ . Then, for the particles moving in positive and negative directions inside the interaction front, their densities  $\rho_+$ ,  $\rho_-$  can be written as

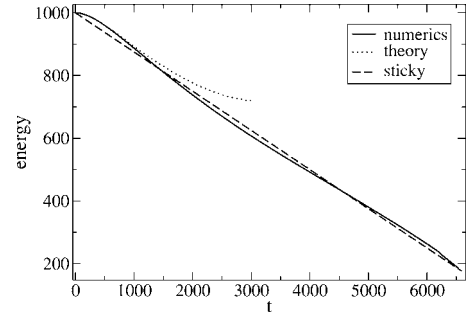


FIG. 4. The energy dissipation in the shock wave in the inelastic gas. The solid line shows the numerical result, the dotted line corresponds to formula (7), and the dashed line represents the sticky gas with the same initial data.  $N=8000$ ,  $u_0=0.5$ .

$$\rho_{\pm}(x, t) = \rho_0 \left( 1 + \frac{[x_f(t) \pm x][u_0 t - x_f(t)]}{2x_f^2(t)} \right), \quad |x| \leq x_f(t).$$

An analogous expression can be written down for the velocities of particles moving in positive and negative directions:

$$u_{\pm}(x, t) = u_0 \left( 1 - \frac{1-\epsilon}{l} [x_f(t) \pm x] \right), \quad |x| \leq x_f(t).$$

Combining the above two expressions we can find an average velocity in the interaction area. In linear approximation, it has a negative slope which does not depend on time:

$$\langle u \rangle(x) = \frac{[tu_0 - x_f(t)] - 2tu_0 x_f(t)(1-\epsilon)/l}{[x_f(t) + u_0 t]x_f(t)} x$$

$$\approx u_0 \ln \left( \frac{1+\epsilon}{2} \right) \frac{x}{l}, \quad |x| \leq x_f(t). \quad (6)$$

Numerical simulations are in a perfect agreement with this estimate [see Fig. 2(b)].

Another important issue for the problem of free cooling is the energy dissipation [14]. In the sticky gas shock wave, it obeys a simple linear relationship,  $E(t) = E(0) - mu_0^3 t / l$ , where  $E(0) = Nmu_0^2 / 2$ . The time dependence of the energy of the shock wave in the inelastic gas is shown in Fig. 4. The early stage can also be described analytically by using the above expressions for the velocity and density of particles:

$$E(t) = E(0) - \frac{2}{3} \rho_0 u_0^2 (1-\epsilon) \frac{x_f(t)}{l}$$

$$\times \left( (1-\epsilon) [3tu_0 + x_f(t)] \frac{x_f(t)}{l} - 2[2tu_0 + x_f(t)] \right). \quad (7)$$

Numerical results confirm this result as well. At the later stage, the numerical energy curve, with decaying oscillations, comes to the sticky limit. This limit follows from the underlying mechanism of large cluster formation in the center of the inelastic shock wave. As its size grows, it becomes an effective sticky center, and thus provides the sticky gas asymptotics.

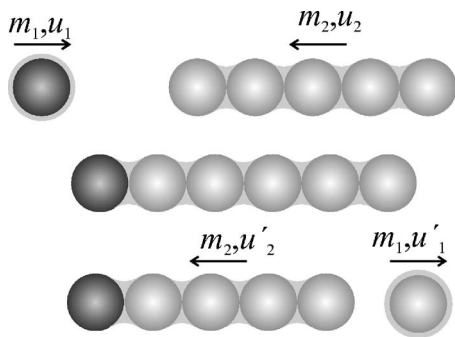


FIG. 5. Particle-cluster interaction in the wet gas. The dark particle hits the cluster from the left. A liquid bridge is formed on the next step instantaneously, and the momentum is transferred to the right most particle of the cluster (like in Newton's cradle). It ruptures the liquid bridge and flies freely. Thus we can interpret this interaction as if the dark particle would pass through the cluster losing the energy required for rupturing the liquid bridge.

In the wet granular gas, the clustering mechanism is different. There is a real sticking of particles into massive solid clusters. The interaction mechanism via the liquid bridge force gives a possibility for the big wet clusters to pass through each other, losing the same fixed  $E_{\text{loss}}$ , unlike the cases of the inelastic or sticky gases. The consequences of these wet gas features will be discussed in the next two sections.

### V. WET GRANULAR GAS

The initial stage of shock development in the wet granular gas is very similar to that of the inelastic gas. However, there are some peculiarities. In a wet gas, our interpretation of particles passing through each other is even more natural. Consider for a moment a big slow cluster of wet particles and one fast particle impinging on it from the left (see Fig. 5). The collision momentum passes through the whole cluster, just as in a Newton cradle, and it tears out a particle on the right side, whereas the particle which initially hit the cluster sticks to its left side. One can imagine it as particles and clusters running through their collision partners and losing a fixed amount of energy. As was done in the previous section, we can find a trajectory of a wet particle with initial velocity  $u_0 > 0$  penetrating into a row of identical particles, but with opposite velocity  $-u_0$ . Its velocity changes between subsequent collisions according to

$$u_{n+1} = \frac{u_n - u_0}{2} + \sqrt{\left(\frac{u_n + u_0}{2}\right)^2 - \frac{E_{\text{loss}}}{m}}.$$

We can rewrite it as a differential equation for  $u(n)$ :

$$\frac{du(n)}{dn} = -\frac{u_0 + u(n)}{2} + \sqrt{\left(\frac{u(n) + u_0}{2}\right)^2 - \frac{E_{\text{loss}}}{m}},$$

where  $n$  again numbers the collision events. This equation can be integrated by separation of variables and gives an implicit dependence  $u(n)$ . We should also mention that our assumption that capillary bridges form instantaneously after

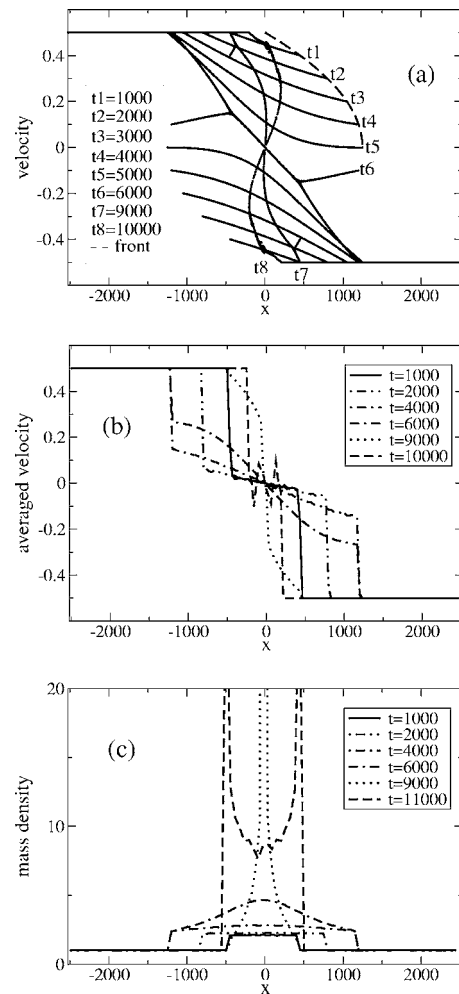


FIG. 6. Simulations of the wet shock wave ( $u_0 = \pm 0.5$ ,  $l = 1$ ,  $N = 50\,000$ , and  $E_{\text{loss}} = 1 \times 10^{-4}$ ). (a) Velocities of particles and the trajectory of the front calculated by Eq. (8). (b) Averaged velocity profiles. (c) The mass density (normalized).

adjacent particles come into contact becomes increasingly justified as the clusters grow. The dynamics of the Newton cradle ensures that contacts remain established for some finite time, leaving capillary bridges ample time to form.

By using familiar expressions for the coordinate increment  $x_n$  during the free flight interval  $t_n$ ,

$$x_{n+1} = x_n + u_n dt_n,$$

$$dt_n = l|u_n + u_0|,$$

we transform it to the corresponding differential equation and find an expression for  $x(n)$ ,

$$x(n) = x_0 + nl - u_0 l \int_0^n \frac{dn}{u(n) + u_0}. \quad (8)$$

In Fig. 6(a) we plot the velocities of particles obtained in the simulations and the trajectory of the first front particle derived from the above results. The implicit character of these expressions does not allow a simple theoretical description of the early stage of the shock formation as in the inelastic

case. Therefore we present mainly numerical results.

In the early stage, the picture of shock formation resembles that of the inelastic gas. Two rows interpenetrate without sticking events, forming two disjoint branches of the velocity profile. Later, when the two velocity branches “come into contact,” they join and form a tree structure [transition between  $t5$  and  $t6$  in Fig. 6(a)]. This is also when the sticking of particles sets in. In Figs. 6(b) and 6(c), the mean velocity and density profiles are shown. The main difference, as compared to the inelastic gas at the early stage, is that the mass density of the wet gas grows in the center of the shock wave rather than at the borders. Note that we must now clearly distinguish between the mass density and the density of clusters.

The buildup of a sharp density maximum at  $x=0$ , as evident from Fig. 6(c), is directly connected to the infinite slope occurring in the velocity profile shown for  $t=9000$  ( $t7$ ) in Fig. 6(a). The peak of the mass density forms when particles which initially penetrated into the opposite rows reverse their motion under the constant pressure from both sides of the shock and are brought back to the center of the shock. However, now these objects (which are going to collide again) have larger masses and inertia. The mass peak splits into two sharp density maxima which recede from the center of the shock. The secondary expansion of the shock is several times wider and not as well-defined as the first one. We can see that the evolution of the wet shock wave is more complex than in the inelastic gas.

However, we can anticipate what will be the asymptotic stage of the process. First of all, we expect that in contrast to the inelastic and sticky gases, the wet shock wave would have a finite (nonzero) width of a collision region where the energy of colliding rows would be dissipated. Any new incoming particle must experience a number of collisions before it becomes slow enough to find a “sticky” partner. The typical deceleration length depends primarily on the density of collision partners. However, in the wet gas there is a growth in the mass of the clusters due to the agglomeration process, rather than the clustering of particles as in the inelastic gas. This property of the wet gas prevents it from having a high (in the inelastic gas: divergent) density of particles. Therefore, due to the finite density of clusters in the wet shock wave, there should be an extended area of interaction of particles with a finite width.

The second prediction is that the mass in the wet shock wave would be accumulated in two symmetric clusters instead of one in the center. It is clear that the particles entering the interaction area would slow down at the opposite side of this area and find their sticky partners there. Thus the mass agglomeration dominates close to the borders of the interaction area, where a number of heavy clusters will start to grow. From momentum conservation, it follows that heavier clusters would have smaller velocities. As the mass of one cluster grows, it demobilizes itself, and captures all other particles with subcritical velocities. Due to the symmetry of the problem, we may anticipate that there will be a pair of large clusters forming. Asymptotically, they accumulate the whole incoming mass, acting as sticky clusters.

Before we present numerical data (which completely corroborates this picture), we will analyze the slow dynamics of

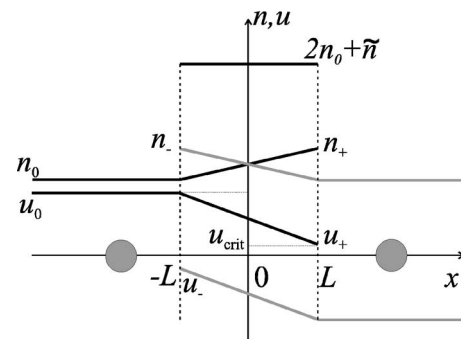


FIG. 7. Linear model for the density and velocity profiles moving in positive ( $n_+, u_+$ ) and negative ( $n_-, u_-$ ) directions. Two gray circles denote two clusters performing oscillatory motion on the fixed background of particles. There are two parameters in the model: width of the dissipation zone,  $L$ , and the density of particles in this zone,  $2n_0 + \tilde{n}$ .

the pair of clusters which form. For this purpose we build a simple toy model which captures the behavior of the density and velocity profiles in the asymptotic regime of the wet shock front. Using these profiles as a background for the motion of the pair of biggest clusters, we predict an oscillatory behavior, which is later confirmed by numerics.

### VI. WET GAS (THEORETICAL TOY MODEL)

Let us set up a linear model of the final stage of the shock wave formation in the wet granular gas. We assume that the density and velocity profiles are stationary. Our main interest is the dynamics of the pair of biggest clusters with growing mass, in particular their motion on the fixed background given by the other particles.

We assume that the particle velocities of the two interpenetrating rows drop linearly and symmetrically (see Fig. 7) from the initial value  $u_0$  to the critical sticking velocity  $u_{crit} = \sqrt{2E_{loss}}/\mu$ . This happens on a spatial scale equal to the width of the interaction area  $2L$ . This spatial scale gives typical starting positions of the pair of big clusters. Denoting by  $u_{\pm}$  the velocities of rows of particles moving in positive and negative directions, inside the interaction zone we can write

$$u_{\pm}(x) = -\frac{u_0 - u_{crit}}{2L}x \pm \frac{u_{crit} + u_0}{2}, \quad |x| < L. \quad (9)$$

For simplicity, we also assume that the particle density behaves linearly, as was done in the inelastic gas (see Fig. 7) (here we use the notation  $n$  for the density of particles in order not to confuse it with the mass density  $\rho$ ):

$$n_{\pm}(x) = \pm \frac{\tilde{n}}{2L}x + \frac{2n_0 + \tilde{n}}{2}, \quad |x| < L. \quad (10)$$

Thus the total particle density in the interaction region is constant and equal to  $2n_0 + \tilde{n}$ , where  $n_0 = l^{-1}$ . There are two unknown parameters in this model: the width of the basic interaction region  $2L$  and the increase of particle density  $\tilde{n}$  in the interaction zone. It is possible to give simple arguments which help to connect these two parameters and even obtain their quantities.

The first equation relating  $L$  and  $\tilde{n}$  can be found from considering the energy balance. The energy flow into the interaction area is given by  $mn_0u_0^3/2$ . The local dissipated energy is equal to the product of the densities of colliding particles and their relative velocity (which in this model is constant and equal to  $u_0$ ):  $E_{\text{loss}}n_+(x)n_-(x)u_0$ . It should be integrated over the whole interaction area. By equating these two quantities we obtain the first equation connecting  $\tilde{n}$  and  $L$ :

$$E_{\text{loss}} \int_0^L n_+(x)n_-(x)u_0 dx = mn_0u_0^3/2. \quad (11)$$

By substituting Eq. (10) in Eq. (11) we find

$$L = \frac{mu_0^2}{2E_{\text{loss}}n_0(k^2/6 + k + 1)}, \quad (12)$$

where  $k = \tilde{n}/n_0$ .

The second way to define the relation between  $\tilde{n}$  and  $L$  is to consider the slowing down of particles from a kinetic point of view. From our assumption that the relative velocity of particles moving in opposite directions is equal to  $u_0$ , we find that the velocity of a particle traveling in positive direction,  $u_+$ , changes between two consecutive collisions  $j$  and  $j+1$  in the following way:

$$u_{+,j+1} = u_{+,j} - \frac{u_0}{2} \left( 1 - \sqrt{1 - \frac{4E_{\text{loss}}}{mu_0^2}} \right) \approx u_{+,j} - \frac{E_{\text{loss}}}{mu_0}.$$

From the above formula, it immediately follows that

$$u_{+,j} = u_0 \left( 1 - j \frac{E_{\text{loss}}}{mu_0^2} \right).$$

Hence the total number of collisions before a particle slows down from  $u_0$  to 0 (actually to  $u_{\text{crit}}$ , however, assuming  $u_{\text{crit}} \ll u_0$ , it can be safely set to zero) is  $j^* = mu_0^2/E_{\text{loss}}$ . For the coordinate change during the deceleration we can write

$$x_{+,j+1} = x_{+,j} + u_{+,j} dt_j, \quad dt_j = 1/n_-(x_{+,j})u_0.$$

Representing the above equation as a differential equation for  $x(j)$  which varies from  $-L$  to  $L$ , we solve it to find

$$L = \frac{mu_0^2}{2E_{\text{loss}}n_0(2+k)}. \quad (13)$$

Comparing Eqs. (12) and (13) we find that  $k = \tilde{n}/n_0 = \sqrt{6} \approx 2.4$ . Substituting this into Eqs. (12) and (13) we can find the dependence of  $L$  on the initial parameters of the problem ( $E_{\text{loss}}$ ,  $u_0$ ,  $n_0$ ). The results agree very well with our numerical data. The two biggest clusters indeed accumulate the whole incoming mass, so that the mass of each cluster grows linearly with time,  $M(t) = mn_0u_0t$ . The density of particles in the interaction zone in the numerics is only several times higher than the initial density of the incoming particles, which agrees with our estimate  $\tilde{n}/n_0 \approx 2.4$ . The width of the interaction area  $2L$ , calculated according to Eqs. (11) and (13), gives the correct scaling with the parameters of the problem ( $u_0$  and  $E_{\text{loss}}$ ). In Fig. 8 we plot the size of the interaction area  $2L$  as a function of the initial parameters  $u_0$  and  $E_{\text{loss}}$

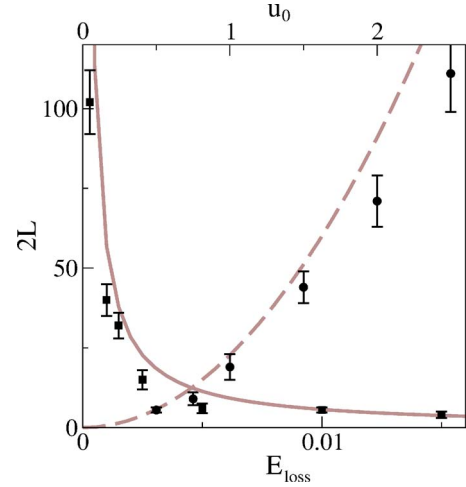


FIG. 8. (Color online) Dependence of the interaction zone width  $2L$  on the initial parameters of the problem  $u_0$  and  $E_{\text{loss}}$ . Circles correspond to the fixed  $E_{\text{loss}}=0.01$  and varying  $u_0$ . Squares are used for the case where  $u_0=0.5$  and  $E_{\text{loss}}$  is changing. Dashed and solid lines correspond to the theoretical predictions of Eq. (13).

following from numerical simulations. In this figure, circles correspond to a fixed  $E_{\text{loss}}=0.01$  and a varying initial velocity of rows  $u_0$ . The corresponding theoretical result (13) is denoted by a dashed line. The square points represent a fixed  $u_0=0.5$  and varying  $E_{\text{loss}}$ , and a solid line shows the prediction of Eq. (13). The overall agreement is quite satisfactory. The large error bars are due to the uncertainty in defining the interaction zone width  $2L$ .

Now we consider slow motion of the massive clusters on the fixed background of particles given by Eqs. (9), (10), (12), and (13). We assume that the mass of the big clusters increases linearly with time  $M(t) = m(1 + u_0n_0t)$ . These clusters represent massive pistons experiencing collisions from both sides. The momentum transferred to the piston depends on the particle velocity  $v$ :

$$\Delta p = v \left( 1 - \sqrt{1 - \frac{2E_{\text{loss}}}{mv^2}} \right).$$

Depending on the piston position, different densities of particles moving in positive and negative directions with different velocities create a net force,  $F_{\Sigma}$ , acting on the piston [see the inset in Fig. 10(b)]:

$$F_{\Sigma}(x) = F_+(x) + F_-(x), \quad (14)$$

where

$$F_{\pm} = \begin{cases} mu_{\pm} \left( 1 - \sqrt{1 - \frac{2E_{\text{loss}}}{mu_{\pm}^2}} \right) u_{\pm} n_{\pm}, & |x| < L \\ 0, & x \geq L \\ \pm n_0 E_{\text{loss}} = \text{const.}, & x \leq -L. \end{cases} \quad (15)$$

Essentially, the force consists of two parts. Inside the interaction region, it is the interplay of particles collisions moving in both directions. Outside this area, the pistons experience a constant force in the direction towards the center of the system only from one sort of particles. To derive its

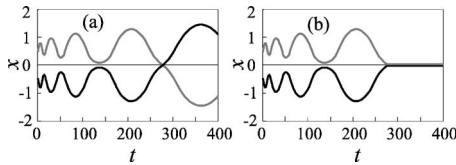


FIG. 9. Two possible scenarios following from Eq. (16). In (a) oscillations starting on both sides of the shock wave increase their amplitude and after collision in the center switch to the second regime of oscillations which then continue indefinitely. In (b) two clusters stick together in the center and oscillations are terminated.

value,  $n_0 E_{\text{loss}}$ , we used the smallness of  $2E_{\text{loss}}/mu_0^2 \ll 1$ . Combining all of the above results, and assuming that the mass of the clusters increases slowly as compared to their oscillatory motion, we are left with a simple equation of motion:

$$m(1 + u_0 n_0 t) \ddot{x} = F_{\Sigma}(x). \quad (16)$$

This equation gives rise to two possible oscillation regimes and two scenarios (see the sketch in Fig. 9). In the first stage each cluster oscillates on one side of the shock wave. The amplitude of these oscillations increases until the clusters meet in the center. At this point, they either switch to a second regime, where the center of the shock wave becomes the center of their symmetric oscillations [first scenario, Fig. 9(a)], or they stick together [second scenario, Fig. 9(b)].

In the second oscillations regime, most of the time the two clusters are outside of the interaction area. There they move under the pressure of new incoming particles. Therefore we can simplify Eq. (16) and search for the scaling relations for the amplitude and frequency of oscillations. A simpler version of Eq. (16) is thus

$$m(1 + u_0 n_0 t) \ddot{x} = -\alpha \operatorname{sgn}(x), \quad \alpha = \text{const.} \quad (17)$$

This equation gives a solution with the following scaling relations. The amplitude of coordinate oscillations grows as  $\bar{x} \propto t^{1/3}$ . The frequency decreases as  $\omega \propto t^{-2/3}$ . From these relations we find that the velocity amplitude decreases as  $\bar{v} \propto t^{-1/3}$  and the energy of the clusters increases as  $\bar{E} \propto t^{1/3}$ . In Fig. 10 we plot the trajectories and velocities of two clusters given by Eq. (16). We intentionally introduced some asymmetry in the growth of the clusters in order to capture the asymmetry appearing in numerical simulations. The mass of the first cluster increases as  $M_1(t) = 1 + 0.45t$ , and the second one as  $M_2(t) = 1 + 0.55t$ . After appropriate tuning of the initial positions and velocities, the clusters will oscillate with the same frequency but different amplitudes (see below).

Let us now turn to the numerical data. In Fig. 11 we plot the trajectories and velocities of the two biggest clusters. The qualitative agreement with the theoretical prediction is obvious. The inset in Fig. 11(a) shows the masses of the two biggest clusters, normalized with respect to the current time. We see that these quantities are close to 0.5 for each cluster. The asymmetry between the clusters is due to the initial perturbations and the threshold character of interaction in the wet gas. In the inset in Fig. 11(b) we show the rescaled velocities of the clusters,  $\tilde{v} := ut^{1/3}$ , according to the scaling

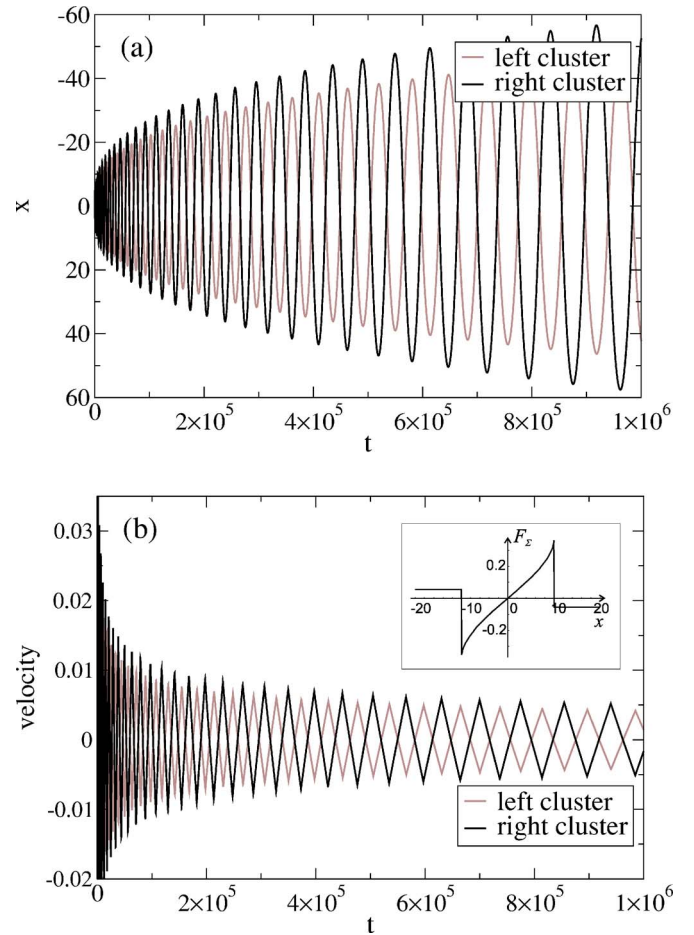


FIG. 10. (Color online) Trajectories (a) and velocities (b) of the two clusters given by Eq. (16) as a function of time. The asymmetry in the clusters' mass growth is introduced:  $M_1(t) = 1 + 0.45t$ ,  $M_2(t) = 1 + 0.55t$ . In the inset in (b) the effective force profile is plotted.

of the theoretical model. As predicted, the amplitude and frequency are constant in this representation. We believe that scaling characteristics are quite robust properties captured by the toy model. As to the asymmetry of oscillation amplitudes, it appears to be strongly dependent on the initial conditions supplied to the model equation. We thus cannot decide at this point whether the striking similarity of numerical and analytical results is a pure coincidence or a meaningful feature of the system.

Here we must mention that there are also two scenarios found in the numerical simulations. Recall that the transition point between oscillation regimes in the theoretical model is marked by the first collision between the biggest clusters in the center. Despite the large mass of these clusters, their relative velocity can be small, so that they just stick to each other. We observe this scenario dominates the numerics. After they stick together, one big cluster drifts to one of the sides of the shock wave, and the second one on the other side starts to grow. The same scenario can be replayed many times. Unfortunately the quality of the numerical data does not provide sufficient statistics to determine for which initial parameters of the problem which type of oscillations would appear in the asymptotics. It should be mentioned that in the

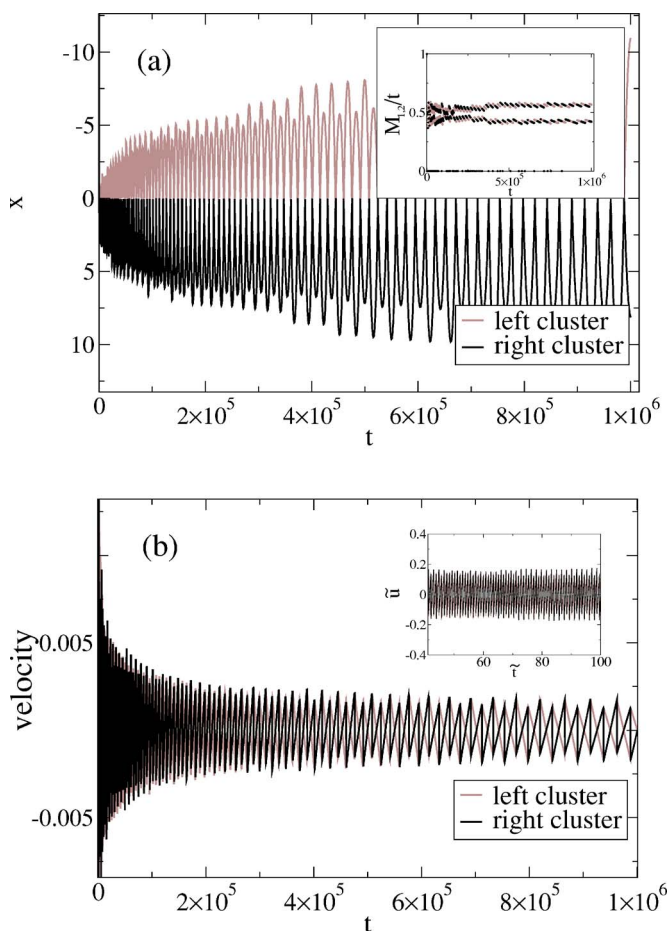


FIG. 11. (Color online) Simulations of the wet shock wave ( $u_0 = \pm 0.5$ ,  $l=1$ ,  $N=2 \times 10^7$ , and  $E_{\text{loss}}=5 \times 10^{-2}$ ). (a) Coordinates of the two biggest clusters as a function of time. In the inset their masses are normalized by the current time,  $M_{1,2}/t$ . (b) Velocities of the two biggest clusters. The inset shows the same plot in rescaled units:  $\tilde{t} = t^{1/3}$ ,  $\tilde{u} = ut^{1/3}$ .

interaction area there exists a cloud of clusters with different masses and nearly zero velocities. This should affect the motion of the pair of clusters as an additional friction force and influence the selection of scenarios.

Relating the above results to the problem of free cooling, we can say that the sticky limit with respect to the energy exists for the wet gas as well. With some decaying oscillations around the sticky limit, the energy curve approaches the latter in the asymptotic regime (not shown). In the case of the wet gas, the sticky asymptotics is provided by the increasing mass of the pair of clusters (with the same rate as in the sticky and inelastic gases), and the deviations from the sticky limit are due to the cloud of clusters in the interaction

area and the energy oscillations of the pair of the biggest clusters. However, the increase of the energy of the clusters is slow ( $\bar{E} \propto t^{1/3}$ ) as compared to the dissipated energy in the interaction area, which is linear in time. Therefore we can say that for the individual shock wave, as previously observed in the free cooling scenario, all three models share the same energy dissipation asymptotics. It is important that on the level of a single shock we can give reasonable arguments why it should be that way.

## VII. CONCLUSIONS

We have demonstrated that for one-dimensional inelastic and wet gases the energy behavior of a single shock wave tends to the sticky limit. In the inelastic gas the asymptotic regime coincides with the sticky solution, but with a huge cluster of correlated particles instead of only one heavy particle in the center. Unexpected features were discovered in the early linear stage of the shock wave development which could be studied analytically. The maximal width of the interaction front was calculated, and the mean velocity and density profiles were obtained. It was shown that the mean velocity profile conserves its negative slope.

We have also shown that the wet granular gas behavior in the asymptotic regime is qualitatively different. It is characterized by a cloud of constant width with slightly higher particle density which is superimposed by two big central clusters. Their masses grow linearly in time as in the sticky limit. The clusters perform a well-defined oscillatory motion with increasing amplitude and decreasing frequency. Our simple theoretical model allowed us to identify the basic processes responsible for this behavior and to find the asymptotic scaling laws for the oscillations.

The similarity in the energy dissipation of the isolated individual shock waves suggests that the macroscopic behavior of a set of such shocks in the free cooling scenario should be also similar for sticky, inelastic, and wet granular gases. The analytical results of this paper may be useful for understanding the early stages of the shock development and for testing the one-dimensional hydrodynamic equations suggested for the description of the dissipative gases. We believe that the qualitative picture of the shock formation obtained in the present paper will help to provide an advanced theoretical description of this process.

## ACKNOWLEDGMENTS

The authors would like to thank M. Brinkmann for his constant support with the numerical simulations and Z. Khan for the help with the manuscript. Intense and fruitful discussions with Professor E. Ben-Naim, Professor K. V. Chukbar, Professor V. I. Oseledec, and A. Fingerle are greatly acknowledged.

- [1] N. V. Brilliantov and T. Pöschel, *Kinetic Theory of Granular Gases* (Oxford Univ. Press, Oxford, UK, 2004).
- [2] N. V. Brilliantov and T. Pöschel, *Granular Gas Dynamics*, Springer Lecture Notes in Physics, Vol. 624 (Springer, Berlin, 2003).
- [3] L. P. Kadanoff, *Rev. Mod. Phys.* **71**, 435 (1999).
- [4] J. Duran, *Sands, Powders and Grains* (Springer, New York, 2000).
- [5] J. W. Dufty, *Recent Res. Dev. Phys.* **2**, 21 (2005).
- [6] A. Barrat, E. Trizac, and M. H. Ernst, *J. Phys.: Condens. Matter* **17**, S2429 (2005).
- [7] I. Goldhirsch, *Annu. Rev. Fluid Mech.* **35**, 267 (2003).
- [8] S. F. Shandarin and Ya. B. Zeldovich, *Rev. Mod. Phys.* **61**, 185 (1989).
- [9] W. E, Ya. G. Rykov, and Ya. G. Sinai, *Commun. Math. Phys.* **177**, 349 (1996).
- [10] L. Frachebourg, *Phys. Rev. Lett.* **82**, 1502 (1999).
- [11] L. Frachebourg, Ph. Martin, and J. Piasecki, *Physica A* **279**, 69 (2000).
- [12] G. F. Carnevale, Y. Pomeau, and W. R. Young, *Phys. Rev. Lett.* **64**, 2913 (1990).
- [13] S. Herminghaus, *Adv. Phys.* **54**, 221 (2005).
- [14] V. Yu. Zaburdaev, M. Brinkmann, and S. Herminghaus, *Phys. Rev. Lett.* **97**, 018001 (2006).
- [15] A. Fingerle and S. Herminghaus, *Phys. Rev. Lett.* **97**, 078001 (2006).
- [16] E. Ben-Naim, S. Y. Chen, G. D. Doolen, and S. Redner, *Phys. Rev. Lett.* **83**, 4069 (1999).
- [17] X. Nie, E. Ben-Naim, and S. Chen, *Phys. Rev. Lett.* **89**, 204301 (2002).
- [18] Y. Brenier and E. Grenier, *SIAM (Soc. Ind. Appl. Math.) J. Numer. Anal.* **35**, 2317 (1998).
- [19] Ya. G. Sinai, *Commun. Math. Phys.* **148**, 601 (1992).
- [20] J. Burgers, *The Nonlinear Diffusion Equation* (Reidel, Dordrecht, 1974).
- [21] N. Sela and I. Goldhirsch, *Phys. Fluids* **7**, 507 (1995).
- [22] R. Ramirez and P. Cordero, *Phys. Rev. E* **59**, 656 (1999).
- [23] S. Serna and A. Marquina, *J. Comput. Phys.* **209**, 787 (2005).
- [24] V. Kamenetsky, A. Goldshtein, M. Shapiro, and D. Degani, *Phys. Fluids* **12**, 3036 (2000).
- [25] N. Sela and I. Goldhirsch, *J. Fluid Mech.* **361**, 41 (1998).
- [26] A. Goldshtein and M. Shapiro, *J. Fluid Mech.* **282**, 75 (1995); A. Goldshtein, M. Shapiro, L. Moldavsky, and M. Fishman, *ibid.* **287**, 349 (1995); A. Goldshtein, M. Shapiro, and C. Gutfinger, *ibid.* **316**, 29 (1996); *ibid.* **327**, 117 (1996).
- [27] B. Meerson and A. Puglisi, *Europhys. Lett.* **70**, 478 (2005).
- [28] E. Efrati, E. Livne, and B. Meerson, *Phys. Rev. Lett.* **94**, 088001 (2005).
- [29] T. Pöschel, N. V. Brilliantov, and T. Schwager, *J. Phys.: Condens. Matter* **17**, S2705 (2005).
- [30] C. Villani, *J. Stat. Phys.* **124**, 781 (2006).
- [31] P. I. Hurtado, *Phys. Rev. Lett.* **96**, 010601 (2006).
- [32] E. Thiesen and W. A. M. Morgado, *Phys. Rev. E* **73**, 051303 (2006).
- [33] I. Goldhirsch and G. Zanetti, *Phys. Rev. Lett.* **70**, 1619 (1993).
- [34] I. Goldhirsch, S. H. Noskowitz, and O. Bar-Lev, *J. Phys.: Condens. Matter* **17**, S2591 (2005).
- [35] Y. Du, H. Li, and L. P. Kadanoff, *Phys. Rev. Lett.* **74**, 1268 (1995).
- [36] F. Bouchut, in *Advances in Kinetic Theory and Computing: Selected papers, Series on Advances in Mathematics for Applied Sciences, Vol.22*, (World Scientific, Singapore, 1994), p. 171.
- [37] E. Hopf, *Commun. Pure Appl. Math.* **3**, 201 (1950).
- [38] G. Whitham, *Linear and Nonlinear Waves* (Wiley, New York, 1974).
- [39] O. Rudenko and S. Soluyan, *Theoretical Foundations of Nonlinear Acoustics* (Plenum Press, New York, 1977).
- [40] Y. Kuramoto, *Chemical Oscillations, Waves and Turbulence* (Springer-Verlag, Berlin, 1985).
- [41] S. Gurbatov, A. Malakhov, and A. Saichev, *Nonlinear Random Waves and Turbulence in Nondispersive Media: Waves, Rays, Particles* (Manchester University Press, Manchester, 1991).
- [42] M. Vergassola, B. Dubrulle, U. Frisch, and A. Noullez, *Astron. Astrophys.* **289**, 325 (1994).